

# In Search of the Hair-Cell Gating Spring: Elastic Properties of Ankyrin and Cadherin Repeats

Marcos Sotomayor,<sup>1</sup> David P. Corey,<sup>2,\*</sup>  
and Klaus Schulten<sup>1,\*</sup>

<sup>1</sup>Department of Physics  
University of Illinois at Urbana-Champaign and  
Beckman Institute for Advanced Science  
and Technology  
Urbana, Illinois 61801

<sup>2</sup>Howard Hughes Medical Institute and  
Department of Neurobiology  
Harvard Medical School  
Boston, Massachusetts 02115

## Summary

Mechanotransduction in vertebrate hair cells involves a biophysically defined elastic element (the “gating spring”) that pulls on the transduction channels. The tip link, a fine filament made of cadherin 23 linking adjacent stereocilia in hair-cell bundles, has been suggested to be the gating spring. However, TRP channels that mediate mechanotransduction in *Drosophila*, zebrafish, and mice often have cytoplasmic domains containing a large number of ankyrin repeats that are also candidates for the gating spring. We have explored the elastic properties of cadherin and ankyrin repeats through molecular dynamics simulations using crystallographic structures of proteins with one cadherin repeat or 4 and 12 ankyrin repeats, and using models of 17 and 24 ankyrin repeats. The extension and stiffness of large ankyrin-repeat structures were found to match those predicted by the gating-spring model. Our results suggest that ankyrin repeats of TRPA1 and TRPN1 channels serve as the gating spring for mechanotransduction.

## Introduction

The vertebrate senses of hearing and balance employ mechanically sensitive hair cells to transform complex mechanical stimuli produced by sound and acceleration into electrical signals. In both the auditory and vestibular systems, these stimuli bend the hair cells' stereocilia, microvillus-like organelles that project in bundles from the apical surfaces of the cells, and the bending opens mechanically gated transduction channels in the tips of stereocilia to allow ion influx (Hudspeth and Corey, 1977; Hudspeth, 1982; Gillespie and Walker, 2001). The biophysics of this process is well understood, and sensitive mechanical measurements have characterized the force needed to open channels and the stiffness of structures that convey this force (Corey and Hudspeth, 1983; Howard et al., 1988). The microscopic structures involved are also well understood: stereocilia in each hair bundle are arranged in rows of increasing height, and a fine filament termed a

tip link connects the tip of each stereocilium to the side of its taller neighbor. Tip links are thought to connect directly to transduction channels, so that deflections of a hair bundle that would tighten tip links open these channels (Pickles et al., 1984; see Figure S1).

In recent years, proteins composing the transduction apparatus have begun to be identified. Myosin-1c, a small, unconventional myosin, is clustered at each end of the tip link; the several dozen myosins in each cluster maintain a tension on channels to set a resting bias so that the channels are poised at their most sensitive point (Gillespie et al., 1993; Garcia et al., 1998; Holt et al., 2002). The tip link is composed in large part of cadherin 23, a long cadherin with 27 extracellular cadherin domains, which may extend from each stereocilium to form an antiparallel dimer or tetramer (Siemens et al., 2004; Söllner et al., 2004; Corey and Sotomayor, 2004). The transduction channel is likely to contain subunits of the TRP channel family (Corey, 2003; Clapham, 2003), perhaps TRPN1 (NOMPC) in lower vertebrates and TRPA1 (ANKTM1) in all vertebrates (Walker et al., 2000; Sidi et al., 2003; Corey et al., 2004).

A challenge at this point is to correlate the biophysically defined properties of the transduction apparatus with the proteins it comprises. For example, the stiffness of an elastic element that pulls on transduction channels (the “gating spring”) has been measured to be about 1 mN/m (Howard and Hudspeth, 1988; D.P.C. and E.L.M. Cheung, unpublished data). This elasticity might reside in the tip-link protein, with its 27 cadherin repeats (Pickles et al., 1984), or it may reside in the extended N termini of TRPN1 and TRPA1 channels, which contain 29 or 17 ankyrin repeats, respectively (Howard and Bechstedt, 2004; Corey and Sotomayor, 2004; Corey et al., 2004). The gating spring appears to have a working extension of 10–20 nm, a maximum extension of 125–250 nm to accommodate large stimuli, and a relaxation time of 10  $\mu$ s or less to follow high auditory frequencies (Corey and Hudspeth, 1983; Howard and Hudspeth, 1988; Holt et al., 2002). Do either cadherin domains or ankyrin repeats possess similar mechanical properties?

Cadherin proteins are typically formed by a single-pass transmembrane domain and multiple extracellular repeats, and play a fundamental role in calcium-dependent cell-cell adhesion. In general, each cadherin repeat consists of about 100 amino acids sharing a common folding topology characterized by seven antiparallel  $\beta$  strands tightly linked by hydrogen bonds. The microscopic architecture of cadherins along with high-resolution electron micrographs (Kachar et al., 2000) suggests that the tip link is actually a rather stiff element.

Ankyrin repeats are 33-amino-acid domains that occur in sets of four or more and appear in more than 400 human proteins expressed in many tissues (Lux et al., 1990a; Lux et al., 1990b; Bork, 1993; Sedgwick and Smerdon, 1999). Each repeat has two short antiparallel  $\alpha$  helices and a less ordered loop, with the helix pairs stacked in parallel in adjacent repeats (Figures 1A and

\*Correspondence: dcorey@hms.harvard.edu (D.P.C.); kschulte@ks.uiuc.edu (K.S.)

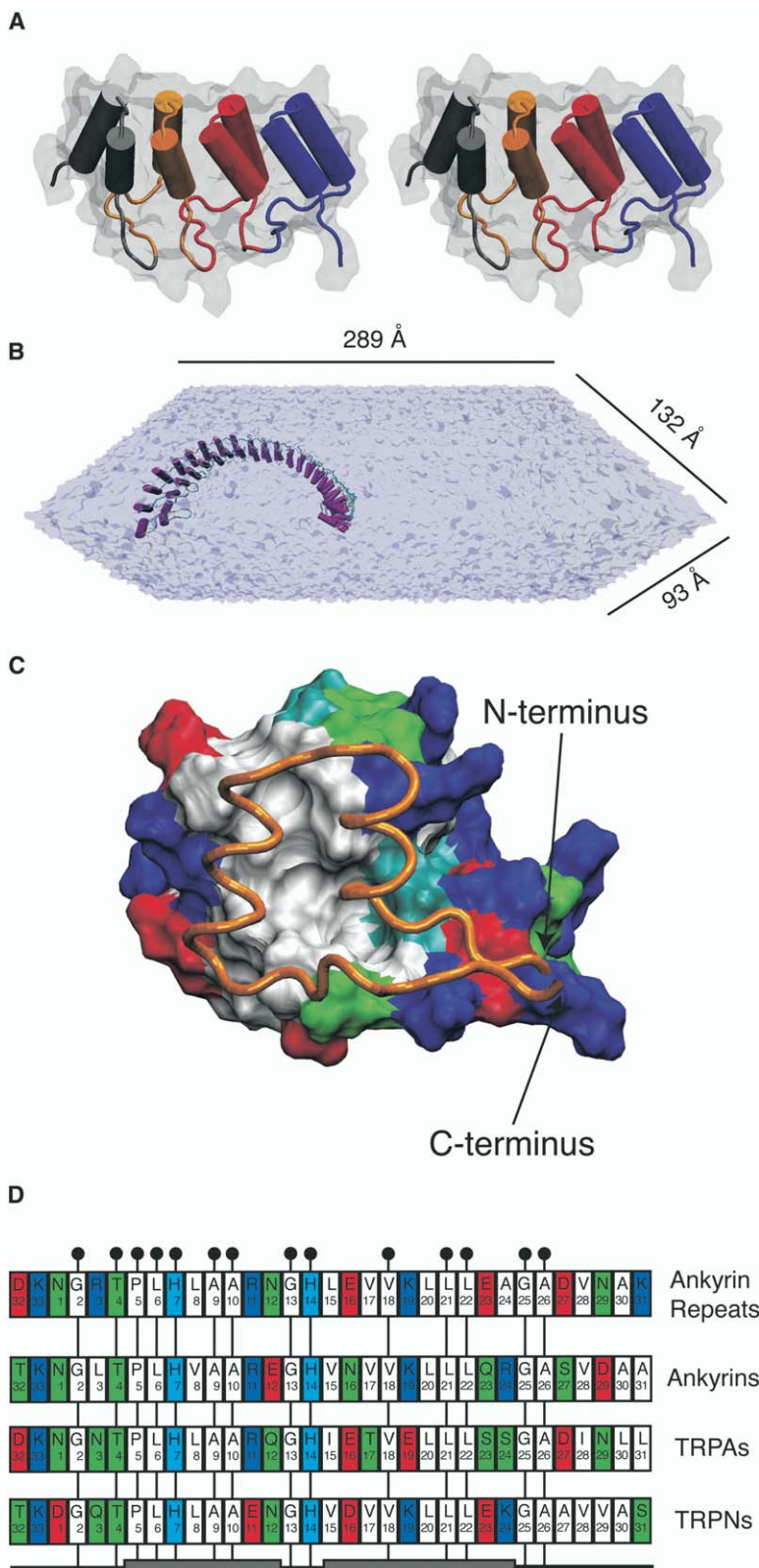


Figure 1. Structure and Sequence of Ankyrin Repeats

(A) Stereo view of four ankyrin repeats (Mosavi et al., 2002) in cartoon representation. Each repeat includes ~33 amino acids that form two  $\alpha$  helices (cylinders) connected by a short linker; adjacent repeats are connected by a longer loop. The four repeats are colored blue (N terminus), red, orange, and gray. The surface of the protein is drawn in transparent gray.

(B) Model of the 24 ankyrin repeats of human ankyrin-R solvated in a water box (339,000-atom system).

(C) Side view of two ankyrin repeats. The two  $\alpha$  helices of the orange repeat in (A) are shown in tube representation. Behind the orange repeat, another repeat (red in [A]) is shown here in surface representation and colored by residue type (white, non-polar residues; blue, basic residues; red, acidic residues; green, polar residues; cyan, histidines). The hydrophobic core of the protein is clearly discernible. N and C termini of the orange repeat are indicated by arrows.

(D) Consensus sequences (color indicates residue type) for all ankyrin repeats (Mosavi et al., 2002), those in ankyrin proteins, those in TRPA channels, and those in TRPN (NOMPC) channels. The position of the  $\alpha$  helices is indicated in gray. Black circles denote highly conserved residues of the ankyrin motif.

1C). Proteins of the ankyrin family, for which the repeat was named, contain up to 24 repeats. The largest ankyrin-repeat crystallographic structure available to date

corresponds to 12 of the repeats from human ankyrin-R, and a structure with 24 repeats was extrapolated from it (Michaely et al., 2002). There is a slight curvature

Table 1. Summary of Simulations

Label	Structure	Type	Size (Å <sup>3</sup> )	Atoms × 1000	Ensemble	Relevant Parameter	Time (ns)	Effort (Ma·ns)
sim1a	1L3W-S <sup>a</sup>	EQ	376 × 65 × 60	129	<i>NpT</i>	—	0.60 <sup>c</sup>	0.07
sim1b	1L3W-S <sup>a</sup>	PCV	362 × 61 × 55	129	<i>NV</i>	0.1 Å/ps	3.00	0.38
sim1c	1L3W-S <sup>a</sup>	PCV	362 × 61 × 55	129	<i>NV</i>	0.01 Å/ps	23.10	2.98
sim2a	1L3W-S <sup>b</sup>	EQ	376 × 65 × 60	129	<i>NpT</i>	—	0.60 <sup>c</sup>	0.07
sim2b	1L3W-S <sup>b</sup>	PCV	362 × 61 × 55	129	<i>NV</i>	0.1 Å/ps	2.90	0.37
sim3a	1N11-S	EQ	199 × 81 × 78	117	<i>NpT</i>	—	0.60 <sup>c</sup>	0.07
sim3b	1N11-S	PCV	192 × 78 × 75	117	<i>NV</i>	0.1 Å/ps	0.75	0.08
sim3c	1N11-S	EQ	192 × 78 × 75	117	<i>NVT</i>	—	5.25	0.61
sim3d	1N11-S	PCF	192 × 78 × 75	117	<i>NV</i>	100 pN	5.00	0.58
sim4a	1N11-S	EQ	419 × 79 × 76	236	<i>NpT</i>	—	0.60 <sup>c</sup>	0.14
sim4b	1N11-S	PCF	405 × 76 × 73	236	<i>NV</i>	250 pN	3.50	0.82
sim4c	1N11-S	PCV	405 × 76 × 73	236	<i>NV</i>	0.1 Å/ps	2.80	0.66
sim4d	1N11-S	PCV	405 × 76 × 73	236	<i>NV</i>	0.1 Å/ps	2.40	0.56
sim5a	MOD1-S	EQ	289 × 93 × 132	339	<i>NpT</i>	—	3.60 <sup>c</sup>	1.22
sim5b	MOD1-S	PCF	281 × 90 × 128	339	<i>NV</i>	25 pN	10.00	3.39
sim5c	MOD1-S	PCF	281 × 90 × 128	339	<i>NV</i>	50 pN	10.00	3.39
sim5d	MOD1-S	PCF	281 × 90 × 128	339	<i>NV</i>	100 pN	1.20	0.40
sim5e	MOD1-S	EQ	281 × 90 × 128	339	<i>NVT</i>	—	24.30	8.23
sim6a	MOD1-V	EQ	—	11	<i>NE</i>	—	3.00 <sup>d</sup>	0.03
sim6b	MOD1-V	EQ	200 × 200 × 200	11	<i>NVE</i>	—	4.00 <sup>d</sup>	0.04
sim6c	MOD1-V	PCF	450 × 200 × 200	11	<i>NV</i>	75 pN	1.00	0.01
sim6d	MOD1-V	EQ	300 × 200 × 200	11	<i>NVE</i>	—	1.50	0.01
sim7a	MOD2-S	EQ	322 × 95 × 92	271	<i>NpT</i>	—	3.50 <sup>c</sup>	0.94
sim7b	MOD2-S	PCF	312 × 92 × 89	271	<i>NV</i>	25 pN	6.50	1.76
sim7c	MOD2-S	PCF	312 × 92 × 89	271	<i>NV</i>	50 pN	6.50	1.76
sim8a	1N0R-S	EQ	352 × 57 × 71	135	<i>NpT</i>	—	1.00 <sup>c</sup>	0.13
sim8b	1N0R-S	PCF	340 × 55 × 69	135	<i>NV</i>	100 pN	21.50	2.90
sim8c	1N0R-S	PCF	340 × 55 × 69	135	<i>NV</i>	200 pN	8.00	1.08
sim8d	1N0R-S	PCF	340 × 55 × 69	135	<i>NV</i>	250 pN	8.00	1.08
sim8e	1N0R-S	PCF	340 × 55 × 69	135	<i>NV</i>	300 pN	3.00	0.40
sim8f	1N0R-S	PCV	340 × 55 × 69	135	<i>NV</i>	0.1 Å/ps	2.40	0.32
sim8g	1N0R-S	EQ	340 × 55 × 69	135	<i>NVT</i>	—	15.60	2.10
sim8h	1N0R-S	PCV	340 × 55 × 69	135	<i>NV</i>	0.01 Å/ps	18.90	2.55

The overall computational effort involved 39 Ma·ns (Million atoms × ns) of simulation (see text). All simulations but one (sim6a) were performed using the particle mesh Ewald method for the computation of long-range electrostatic interactions. Structures are labeled with the corresponding PDB code where applicable, and with MOD for modeled structures. S denotes structures solvated in water and V denotes vacuum simulations; EQ, PCV, and PCF denote equilibration, constant velocity, and constant-force SMD simulations, respectively. Ensembles are denoted according to the thermodynamic quantity held constant (*N*, number of particles; *p*, pressure; *T*, temperature; *V*, volume; *E*, energy). Results of vacuum simulations are discussed in the [Supplemental Data](#).

<sup>a</sup>The structure simulated corresponds to the EC2 domain, including crystallographic ions.

<sup>b</sup>The structure simulated corresponds to the EC2 domain, without crystallographic ions.

<sup>c</sup>These simulations consisted of 1000 steps of minimization, 100 ps of dynamics with the backbone of the protein restrained ( $k = 1$  Kcal/mol/Å<sup>2</sup>), and the remaining time as free dynamics.

<sup>d</sup>These simulations consisted of 100 steps of minimization and the remaining time as free dynamics.

to the stacking, so that 25–30 repeats form a superhelical structure with a complete turn as shown in [Figure 1B](#) ([Michaely et al., 2002](#); [Groves and Barford, 1999](#); [Kajava, 2002](#); [Main et al., 2003](#)). Different ankyrin repeats within a single protein or in different proteins have a rather conserved, but not identical, amino acid sequence. The consensus sequence for various types of ankyrin repeats is shown in [Figure 1D](#). Multiple highly conserved amino acids are involved in stabilizing the structure through hydrogen bonds within each repeat and between adjacent units (see [Supplemental Data](#)). The structure also features a conserved hydrophobic core formed by residues located in positions 6, 9, 10, 17, 18, 20, 21, and 22 (see [Figure 1D](#) and [Figure S5](#)). A less conserved loop linking adjacent repeats mediates protein-protein interactions in some proteins with ankyrin repeats ([Sedgwick and Smerdon, 1999](#); [Bennett and Chen, 2001](#); [Mosavi et al., 2004](#)).

Here we use steered molecular dynamics (SMD) ([Isralewitz et al., 2001a](#)) to ask if either cadherin domains

in the tip link or polyankyrin domains in the transduction channel have elastic properties consistent with the biophysically defined gating spring. We find, first, that individual cadherin domains are very stiff for small forces, and that forces of hundreds of piconewtons cause their complete unfolding. On the other hand, stacks of 12–24 ankyrin repeats form a molecular spring that is reversible on a nanosecond timescale and has a stiffness very close to that of the gating spring. Moreover, forces just above the working range cause unpacking of helices to extend the protein by nearly 10-fold, which may serve as a safety release. We suggest that the ankyrin repeats of TRPA1 and TRPN1 serve as the gating spring for hair-cell mechanotransduction.

## Results

The following section is based on the simulations summarized in [Table 1](#). Details of these simulations are given in [Experimental Procedures](#).

### Elastic Response of Cadherin

In general, cadherin repeats consist of about 110 amino acids sharing a common folding topology, as shown by structure-based sequence analysis (Shapiro et al., 1995) and recent X-ray structures (Boggon et al., 2002). The main component of the tip link, cadherin 23, is made of 27 immunoglobulin-like repeats. No crystal structure of any of the 27 repeats is available to date. However, the structure of five extracellular repeats of the C-cadherin ectodomain is available at 3.1 Å resolution (Boggon et al., 2002). Sequence analysis revealed that the second domain (EC2) of C-cadherin is most similar in sequence (34% homology) to the consensus sequence of cadherin 23. Although the elastic properties of the tip link will certainly depend on many different structural details (dimerization, specific sequences, interdigititation, etc.; see, for instance, Zhu et al., 2003), its elastic response should be mainly determined by the elastic response of individual repeats, because the straight geometry expected of cadherin 23 (Corey and Sotomayor, 2004) distributes applied strain in parallel with each repeat (in contrast, the helical geometry of ankyrin distributes strain to angular interrepeat degrees of freedom). The general architecture of the C-cadherin repeats is characterized by a “Greek key” motif formed by seven antiparallel  $\beta$  strands forming two  $\beta$  sheets and a highly conserved calcium binding motif.

Following earlier work (Bayas et al., 2004), we have performed several simulations of the EC2 domain in order to see if the microscopic elastic response of this cadherin module is compatible with the gating-spring model of mechanotransduction. The structure of the C-cadherin EC2 domain (1L3W), including crystallographically resolved  $\text{Ca}^{2+}$  ions, was stretched in a constant-velocity SMD simulation (Figure 2A; sim1b,  $v = 0.1$  Å/ps). The force versus end-to-end distance graph features three force peaks of  $\sim 2240$  pN,  $\sim 2050$  pN, and  $\sim 850$  pN. The unfolding pathway is shown in Figures 2B–2H. First,  $\beta$  strands G and F (ochre and purple) detached from the structure; followed by  $\beta$  strands D and E (green); and finally  $\beta$  strands C, B, and A (tan, orange, and blue). The  $\text{Ca}^{2+}$  ions were found to interact with highly conserved residues that stabilize the structure, likely causing the observed force peaks. Indeed, detachment of strands G and F required, besides the breakage of hydrogen bonds among  $\beta$  strands, the rupture of a bridge formed by residue Asp134, a  $\text{Ca}^{2+}$  ion, and residue Asp195 (Figure 2D). The detachment of  $\beta$  strands D and E required the rupture of the bridge formed by residue Glu119, a  $\text{Ca}^{2+}$  ion, and residue Asp180 (Figure 2F). Finally, detachment of  $\beta$  strands C, B, and A required the rupture of the bridge formed by residue Asp103, a  $\text{Ca}^{2+}$  ion, and residue Asp136 (Figure 2G). All of these residues are highly conserved not only in C-cadherin but in almost all 27 domains of cadherin 23 as well. The same unfolding pathway was observed during a constant-velocity SMD simulation at one-tenth the rate ( $v = 0.01$  Å/ps) with force peaks of  $\sim 1550$  pN,  $\sim 1350$  pN, and  $\sim 450$  pN (sim1c, data not shown). The observed detachment and unfolding of one  $\beta$  sheet while the other remains partially folded resembles the unfolding pathway predicted for fibronectin type III<sub>1</sub> (Gao et al., 2003) and experimentally confirmed by Li et al. (2004). The elastic response of cadherin was found

to be characterized by little change in the end-to-end distance unless forces of several hundred piconewtons are applied to unfold the domain (data not shown). How does this response depend on the presence of calcium ions? The structural relevance of  $\text{Ca}^{2+}$  ions was further tested in additional simulations in which the ions were not present. An alternative unfolding pathway showing two force peaks of significantly smaller magnitude was observed (Figure 2A and Supplemental Data).

The characteristic sawtooth pattern and the magnitude of the unfolding force peaks observed for the EC2 cadherin domain with or without  $\text{Ca}^{2+}$  ions present seem to be incompatible with the elastic properties of the gating spring. First, the gating spring should be able to elongate over 100 Å, whereas cadherin modules seem to require unphysiologically large forces to unfold and thus provide the required extension. Moreover, the slow refolding timescale may be incompatible with a gating-spring function of domains undergoing repeated unfolding-refolding cycles. Second, the gating spring should be a soft elastic element ( $k \sim 1$  mN/m), while individual cadherin modules show extreme stiffness during constant-force SMD simulations (data not shown). However, whether a rearrangement of 27 tip-link cadherin modules provides softer elasticity without requiring unfolding of individual modules is a question that remains open. Indeed, the crystal structure of five C-cadherin ectodomains (Boggon et al., 2002) shows a significant curvature that is reduced in simulations applying weak stretching forces (data not shown). How this behavior affects cadherin elasticity needs to be further investigated using structural data of tip-link cadherin 23 currently unavailable.

### Response of Polyankyrin Domains to Small Forces

In this section we attempt to answer the question of whether ankyrin repeats are good candidates for the gating spring in mechanotransduction. For this purpose we use simulations of several ankyrin systems.

#### Twelve Ankyrin Repeats of Human Ankyrin-R

The elastic response of the largest crystal structure available of a stack of ankyrin repeats (1N11) to small forces was monitored through its end-to-end distance. A constant-force (100 pN) SMD simulation (Figure 3A; sim3d) revealed that the end-to-end distance increased from  $\sim 86$  Å up to  $\sim 150$  Å, a value that was rather stable over the last  $\sim 2$  ns of the simulation. The overall secondary structure of the protein did not change significantly, but the curvature observed for the initial conformation of the 12-repeat stack did decrease during the simulation. The spring constant corresponding to the mechanical model that best matched the curve was  $k = 16.4$  mN/m (see Experimental Procedures and Table 2). The associated friction constant  $\gamma = 12.71$  pNs/m compares roughly with the friction constant  $\gamma \sim 60$  pNs/m for a globular protein of diameter 6 nm and mass  $m \sim 100$  kDa at 20°C (Creighton, 1993; Howard, 2001). However, the mechanical model did not reproduce well the end-to-end distance at early stages of the simulation (less than 0.5 ns).

#### Twenty-Four Ankyrin Repeats of Human Ankyrin-R

The stack of 24 ankyrin repeats of human ankyrin-R (e.g., MOD1, see Table 1) has been predicted to form a

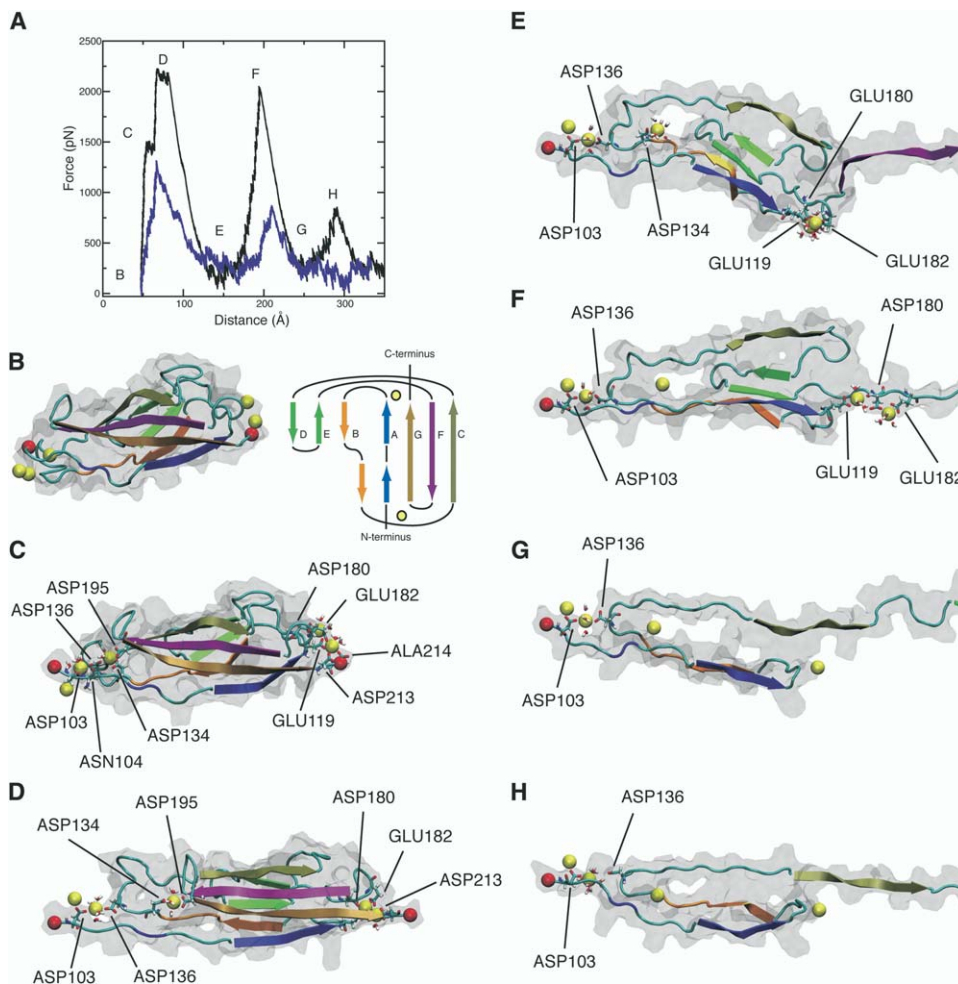


Figure 2. Unfolding of One Cadherin Domain

(A) Force versus end-to-end distance for constant-velocity stretching, with crystallographic Ca<sup>2+</sup> ions (black, sim1b) or without (blue, sim2b). (B) Initial structure and topology of the EC2 C-cadherin ectodomain. The seven β strands (A–G) are shown as thick arrows and are colored blue, orange, tan, green (D and E), purple, and ochre. The positions of Ca<sup>2+</sup> ions are indicated by yellow circles. C<sub>α</sub> atoms of the termini are shown as red spheres and Ca<sup>2+</sup> ions as yellow spheres.

(C–H) Snapshots of the unfolding pathway for one cadherin domain, including crystallographic ions. The views show the EC2 domain of C-cadherin in cartoon representation (same as in [B]) using the secondary structure of the unstretched protein. Specific residues and water molecules surrounding the Ca<sup>2+</sup> ions are labeled and shown in licorice representation.

superhelical structure that may be even more compliant than the stack of 12 ankyrin repeats in ankyrin 1N11. Two constant-force SMD simulations were carried out to probe the elastic response of MOD1 to small forces. The chosen forces (Figure 4A; 25 pN in simulation sim5b and 50 pN in simulation sim5c) are close to those exerted on hair-cell transduction channels for medium and large stimuli. The end-to-end distance during the 25 pN stretch SMD simulation increased from ~112 Å to a rather stable value of ~168 Å within 10 ns of simulation. The overall extension of ~56 Å was found to be caused by a change in the curvature of the structure. No loose loops were present at the ends of the protein, and neither unfolding nor detachment of individual repeats was observed. Moreover, there were no significant changes in the secondary structure of different repeats (see Figures 4B and 4C and Figures S3Aa and S3Ab). The end-to-end distance of the corresponding

mechanical model closely followed the observed end-to-end distance over the whole trajectory and corresponds to a spring constant of  $k = 4.08$  mN/m. The end-to-end distance during the 50 pN SMD simulation (Figure 4A; sim5c) showed a similar behavior, and the mechanical model matching the simulated end-to-end distance corresponds to a spring constant of  $k = 4.72$  mN/m. In both simulations, an increase in the temperature of the system of up to  $\Delta T = 28$  K was observed due to deposition of energy in the protein through stretching. This temperature increase is shared with the solvent surrounding the protein and may also affect the value of the estimated spring constants.

The overall extension in the 50 pN stretch was again caused by a change in curvature. The front and side views of the structure at the end of the simulation (Figure 4D) illustrate the dramatic effect of the rather small external force on the spatial conformation of the pro-

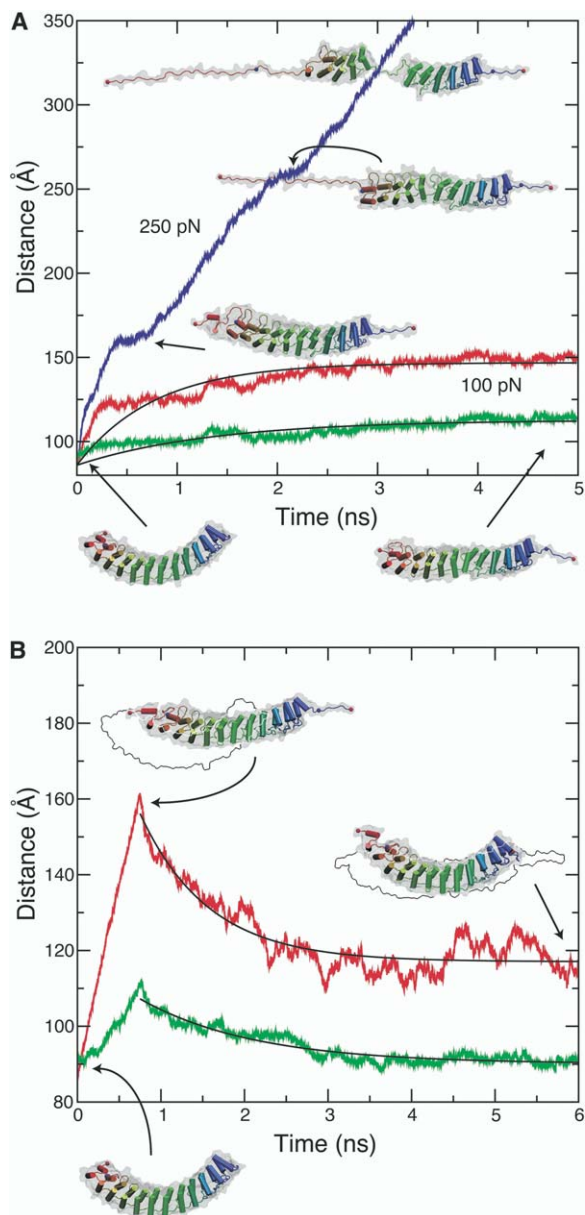


Figure 3. Elastic Response of 12 Ankyrin Repeats in Water

(A) The end-to-end distance is shown for two constant-force SMD simulations (sim3d and sim4b; see Table 1) performed on the solvated crystal structure of 12 ankyrin repeats (13–24) of human ankyrin-R (Michaely et al., 2002). The N terminus of the protein was fixed while the C terminus was stretched with a force of 100 pN (red, sim3d) and 250 pN (blue, sim4b). The distance between  $C_{\alpha}$  atoms of residues Pro430 and Thr780 (see Figure S3B) is shown in green for the 100 pN stretching (sim3d). The initial and final conformations of the structure (without water molecules) for the 100 pN stretching are shown at the bottom in cartoon representation. Repeats are color coded according to their numbering, repeat 13 red and repeat 24 blue. The surface of each structure is shown in transparent gray. Intermediate and final structures for the 250 pN stretching are shown within the plot.

(B) Stretching and relaxation of 12 ankyrin repeats for a constant-velocity stretch (sim3b) and the subsequent release at constant temperature (sim3c). The end-to-end distance is in red and the distance between  $C_{\alpha}$  atoms of residues Pro430 and Thr780 is in green. The initial (equilibrated), elongated, and final (relaxed) conforma-

tein. In particular, the natural twist of each repeat relative to the preceding one was increased during the stretch. Remarkably, the secondary structure of ankyrin seems to be compatible with such drastic changes. Unfolding or detachment of individual repeats was not observed in either case (25 pN or 50 pN).

The predicted spring constants for the 24-ankyrin-repeat structure are clearly smaller than for the 12-ankyrin-repeat structure. Although elongation through reduction of curvature was observed for both structures, the number of ankyrin repeats determined the stiffness of the stack: the larger the number of repeats, the softer the elastic response.

#### Seventeen Ankyrin Repeats of mmTRPA1

The simulations described above indicate that a large stack of ankyrin repeats responds to small forces by changing its curvature. However, neither of the structures mentioned above corresponds to the polyankyrin domains in TRP channels that mediate mechanotransduction processes. Is the elastic response of ankyrin domains located in TRP channels the same as for human ankyrin-R? We studied the elastic response to small forces of a model of the 17 ankyrin repeats (MOD2) of mmTRPA1, recently suggested as part of the mechanotransduction apparatus in mammals (Corey et al., 2004).

Following model building and equilibration (see Experimental Procedures), two constant-force SMD simulations (Figure 5B; sim7b and sim7c) were performed. During simulation sim7b, the protein model (MOD2) was stretched using a constant force of 25 pN. The end-to-end distance increased from  $\sim 117$  Å to  $\sim 186$  Å. The elongation was caused both by changes in the curvature and by extension of loose loops at the ends of the structure. In order to isolate the effect of the latter, the distance between  $C_{\alpha}$  atoms of residues Pro5 and Phe579 was computed. In this case the mechanical model reproduced the elongation process accurately for a spring constant of  $k = 5.96$  mN/m. In simulation sim7c, the protein was stretched with a constant force of 50 pN. The end-to-end distance behavior and the conformational changes were similar to the previous case (Figures 5D and 5E). The distance between  $C_{\alpha}$  atoms of residues Pro5 and Phe579 is reproduced by a mechanical model with  $k = 8.33$  mN/m. The spring constant obtained for 50 pN is  $\sim 40\%$  larger than for a force of 25 pN, indicating a greater nonlinearity than in the case of MOD1.

During the simulation of MOD2 we observed that residue Pro333 breaks the second helix of repeat 10. Orientation and curvature of the MOD2 backbone changed near repeat 10, but packing of the repeats was conserved. A calcium binding EF motif formed by the loops between repeats 12 and 13 was also identified. Whether these particular features of the ankyrin domain of TRPA1 are relevant for its mechanical function remains to be elucidated.

tions are shown as in (A). The contour of each preceding configuration is depicted by a solid line. Solid black curves in (A) and (B) represent results for models of an overdamped spring of negligible mass (see text and Table 2).

Table 2. Parameters Used in Simple Mechanical Models of Ankyrin Repeats

Label	Mass (kDa)	$\gamma$ (pNs/m)	$k$ (mN/m)	$\tau$ (ns)	$x_0$ (Å)	$l$ (Å)	$F$ (pN)
sim3d <sup>a</sup>	—	12.71	16.4	0.775	86	—	100
sim3d <sup>b</sup>	—	50.47	37.2	1.364	86	—	100
sim3c <sup>a</sup>	—	—	—	0.815	117	39	—
sim3c <sup>b</sup>	—	—	—	1.371	90	17	—
sim5b	—	11.48	4.08	2.813	112	—	25
sim5c	—	10.77	4.72	2.279	112	—	50
sim5e	—	—	—	3.098	158	30	—
sim6c	22.1	1.01	15.30	0.066	140	—	75
sim6c <sup>c</sup>	22.2	0.30	16.08	0.018	140	—	75
sim6d	31.7	0.20	15.70	0.013	150	43	—
sim7b <sup>a</sup>	—	5.53	3.58	1.544	117	—	25
sim7b <sup>d</sup>	—	7.99	5.96	1.340	109	—	25
sim7c <sup>a</sup>	—	9.09	5.44	1.671	117	—	50
sim7c <sup>d</sup>	—	12.75	8.33	1.530	109	—	50
sim8g	—	—	—	3.668	91	98	—

Equations 4, 5, 6, and 7 were used along with the parameters shown to fit the corresponding end-to-end distances observed in simulations denoted as in Table 1. Results of vacuum simulations are discussed in the Supplemental Data. As a reference, the friction (drag) coefficient  $\gamma$  for a globular protein at 20°C, diameter 6 nm, and mass  $m \sim 100$  kDa is  $\gamma \sim 60$  pNs/m (Creighton, 1993; Howard, 2001), the total mass of 24 repeats of human ankyrin-R is  $m \sim 83$  kDa, and the estimated gating-spring constant in models of mechanotransduction is  $\sim 1$  mN/m (Howard and Hudspeth, 1988).

<sup>a</sup>End-to-end distance was modeled.

<sup>b</sup>Distance between  $C_{\alpha}$  atoms of residues Pro430 and Thr780 was modeled.

<sup>c</sup>The value of the drag coefficient in this case was restricted to be less than 0.30 pNs/m.

<sup>d</sup>Distance between  $C_{\alpha}$  atoms of residues Pro5 and Phe579 was modeled.

The three proteins investigated, containing 12, 24, and 17 ankyrin repeats, all responded to small forces by changing their curvature rather than by unfolding their individual repeats. Sequences are not identical for repeats within one protein or between different proteins; thus, the elastic response to small forces may be a general property of polyankyrin domains.

#### Elastic Relaxation of Polyankyrin Domains after Stretch

Is the deformation of polyankyrin domains reversible? We performed multiple simulations where we explored the reversibility of the deformation induced by small forces on 12- and 24-ankyrin-repeat structures.

Two simulations (Figure 3B; sim3b and sim3c) were performed for the 12-ankyrin-repeat case. First, the structure 1N11 was stretched at constant velocity ( $v = 0.1$  Å/ps; sim 3b) for 0.75 ns. Then, velocities of all atoms in the system were randomly reinitialized and the system was permitted to relax without force applied for 5.25 ns at constant temperature ( $T = 300$  K, all constraints eliminated; sim3c). The end-to-end distance of the protein increased from  $\sim 86$  Å to  $\sim 161$  Å with force applied, and then decreased to  $\sim 117$  Å with force released (Figure 3B). The  $\sim 45$  Å decrease in the end-to-end distance demonstrates clearly that elongation under stretching, characterized by a curvature change, is partially reversible in a surprisingly short time ( $\sim 5$  ns). However, the end-to-end distance did not decrease entirely to its original value, likely due to distortions in the loose ends. The average radius of curvature increased from an initial value of  $\bar{R} \sim 44$  Å to  $\bar{R} \sim 71$  Å at the end of the constant-velocity SMD simulation and then relaxed to  $\bar{R} \sim 54$  Å. Furthermore, rmsd values (see Figure S2B) reveal that the protein also recovered its initial local structure in 5 ns. The mechanical model that

best matched the overall end-to-end distance involved a relaxation time  $\tau = 0.815$  ns, consistent with the model parameters for the simulation sim3d (Figure 3B;  $\tau \sim \gamma/k$ , see Table 2). To the best of our knowledge, this is one of the first studies where a reversible protein extension has been seen in a molecular dynamics simulation (see also Li et al., 2001).

Is the deformation induced by small forces also reversible for the 24-ankyrin-repeat structure? Two simulations of MOD1 were performed to answer this question (Figure 4E; sim5d and sim5e). During the first simulation (1.2 ns) the structure was stretched using a constant force of 100 pN. Then, velocities of all atoms were randomly reinitialized and the system was equilibrated for 24.3 ns at  $T = 300$  K with all constraints eliminated. The end-to-end distance (Figure 4E) increased from  $\sim 112$  Å to  $\sim 193$  Å and then decreased to  $\sim 151$  Å. The overall decrease of  $\sim 42$  Å is remarkable and in this case cannot be explained by movement of loose ends. As for the 12-ankyrin-repeat structure, the overall curvature of MOD1 was reduced during the constant-force SMD simulation and then partially recovered during the relaxation (Figures 4F–4H). The twist of one repeat with respect to the preceding one also showed an increase and subsequent recovery. Again, the secondary structure of this protein model (MOD1) did not show significant changes during the stretching simulation or the  $\sim 24$  ns relaxation (Figures S3Ad and S3Ae). Although the mechanical model does match the overall behavior of the end-to-end distance during relaxation, there are clear signs of richer dynamics involving multiple modes of oscillation (Figure 4E).

These results indicate that deformations induced by small forces on 12 and 24 ankyrin repeats of human ankyrin-R are highly reversible, even on short time-scales. However, equilibration of the elongated MOD2 model containing the 17 ankyrin repeats of TRPA1

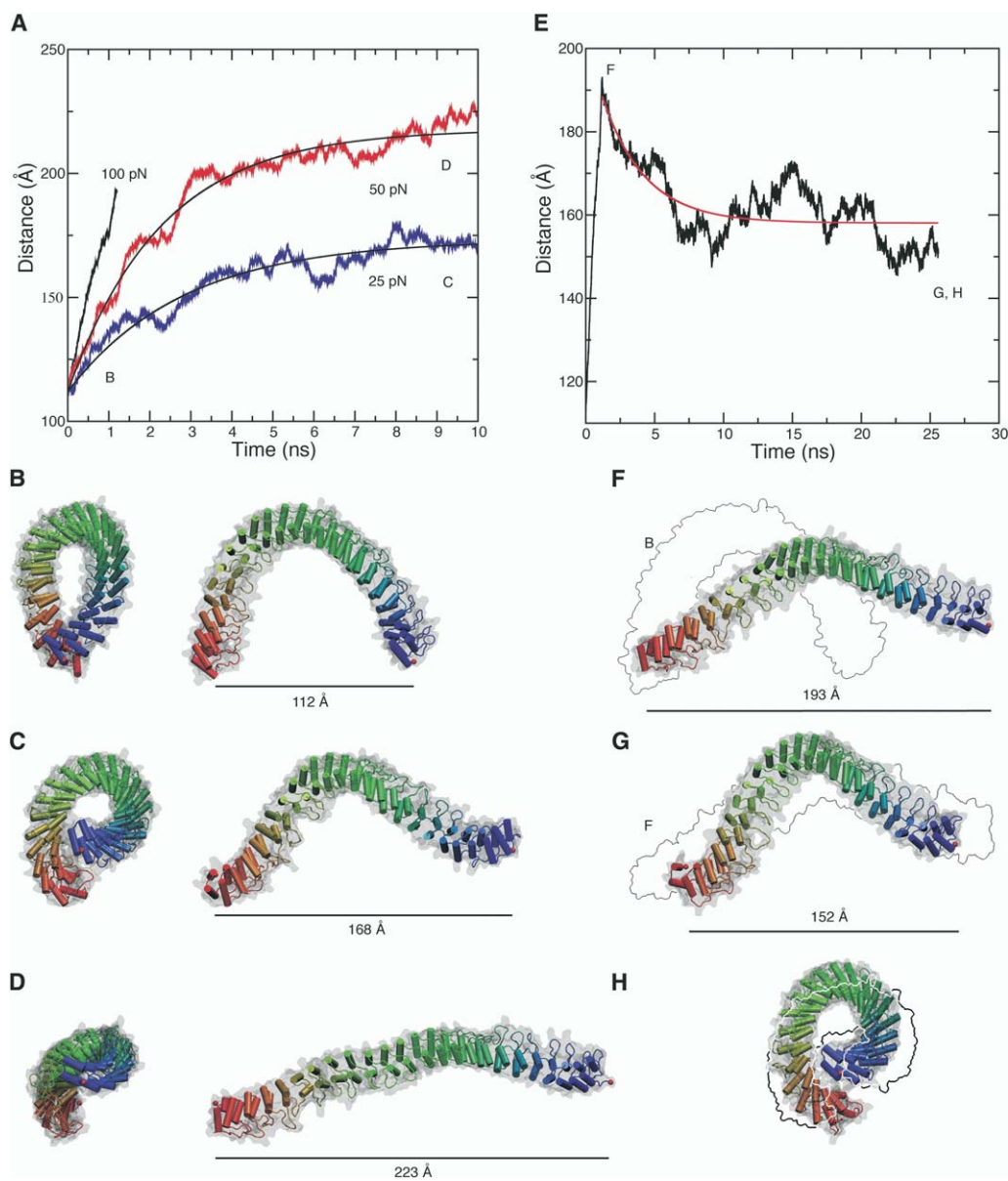


Figure 4. Elastic Response of 24 Ankyrin Repeats in Water

(A) End-to-end distance for two constant-force SMD simulations performed on the solvated and equilibrated (sim5a) model of all 24 repeats of human ankyrin-R (Michaely et al., 2002). The N terminus of the protein was fixed while the C terminus was stretched with forces of 25 pN (blue, sim5b) and 50 pN (red, sim5c). Solid black curves represent results for models of an overdamped spring of negligible mass (see text and Table 2).

(B) Front and side views of the initially equilibrated 24-repeat structure (sim5a).

(C and D) Snapshots of the 24-repeat structure at the end of constant-force simulations using forces of 25 pN and 50 pN.

(E) End-to-end distance for constant-force stretching (100 pN for 1.2 ns, sim5d) and subsequent relaxation for the 24 repeats of human ankyrin-R (~24 ns, sim5e). The red curve represents a model assuming a massless overdamped spring.

(F) Side view of the 24-repeat structure elongated after applying a 100 pN constant force for 1.2 ns (sim5d). The contour of the initial configuration (as in [B]) is depicted by a solid black line.

(G) Side view of the 24-repeat structure after ~24 ns of relaxation (sim5e) as shown in (E).

(H) Front view of the structure after relaxation; different view of (G). The contour of the elongated structure in (F) is depicted by a black line in (G) and (H). Repeats are color coded according to their numbering, repeat 1 red and repeat 24 blue. The surface of the protein is transparent gray.

showed little recovery of its end-to-end distance, at least over 5 ns (data not shown). Perhaps the presence of extra residues (loops) and a more heterogeneous sequence are responsible for this difference in elastic response.

#### Response of Polyankyrin Domains to Large Forces

The simulations mentioned above described the elastic behavior of stacks of 12, 17, and 24 ankyrin repeats when stretched using relatively small forces. What is the response of polyankyrin domains to larger forces?

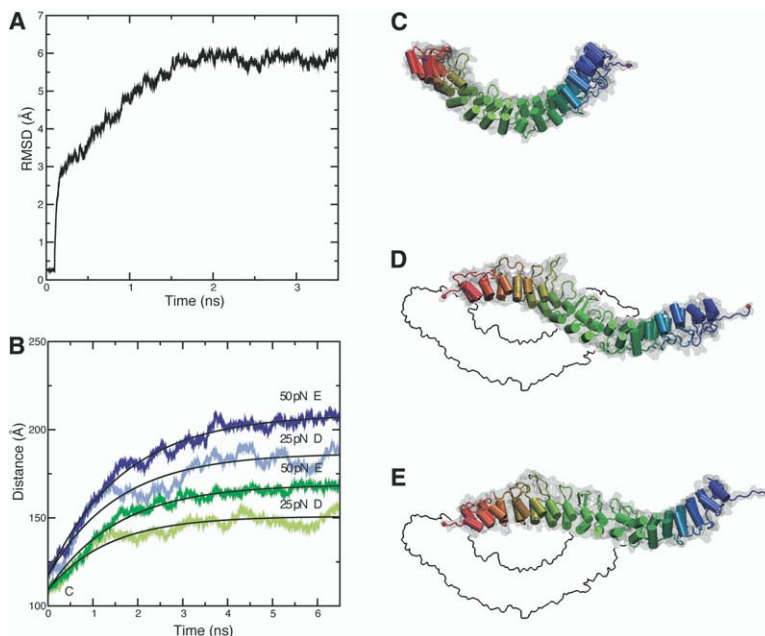


Figure 5. Model of TRPA1 (ANKTM1) Ankyrin-Repeat Domain

(A) Root-mean-square deviation (rmsd) with respect to the initial modeled structure during 3.5 ns of equilibration (sim7a).

(B) End-to-end distance during constant-force stretching (light blue, 25 pN, sim7b; blue, 50 pN, sim7c). Distance between  $C_{\alpha}$  atoms of Pro5 and Phe579 (light green, 25 pN, sim7b; green, 50 pN, sim7c). Solid black curves represent mechanical models assuming an overdamped spring behavior (see text and Table 2).

(C) Equilibrated structure of 17 TRPA1 ankyrin repeats; repeats are color coded according to numbering, the first red and the last blue.

(D and E) Snapshots of 17 TRPA1 ankyrin repeats at the end of constant-force SMD simulations using 25 and 50 pN as in (B) (sim7b and sim7c, respectively). The contour of the initial configuration (as in [C]) is depicted by a solid black line.

To answer this question, we stretched 1N11 with 12 ankyrin repeats, applying a 250 pN force (Figure 3A; sim4b). The structure showed a first stage of elongation similar to that in the 100 pN simulation (sim3d), and then a second stage, in which unfolding and defragmentation of the structure occurred. During stage one the end-to-end distance increased from  $\sim 86$  Å to  $\sim 162$  Å; repeat 13 slightly detached from repeat 14, the overall structure decreased its curvature, and the loose loop at the end of repeat 24 became completely unfolded. The plateau in the end-to-end distance at  $\sim 162$  Å marks the end of this stage (Figure 3A). During stage two, repeat 13 unfolded, extending the structure to  $\sim 260$  Å. The end-to-end distance briefly plateaued, but then repeat 18 separated from repeat 19. The structure actually broke at this point, and two separated stacks of ankyrin repeats were observed before further unfolding occurred (Figure 3A). The breakdown of the stack into two pieces seems to be compatible with proteolytic maps that suggest the existence of four smaller domains of six ankyrin repeats each in the human ankyrin-R protein (Michaely and Bennett, 1993).

When the 1N11 structure was stretched at constant velocity (sim4c and sim4b; see Figure S2A), forces involved in the first stage of elongation ranged up to 200 pN, whereas the second stage of elongation, involving unfolding and detachment of repeats, generated 300–400 pN forces. The range of the forces observed, however, may not be accurate, since the velocity assumed ( $v = 0.1$  Å/ps) is several orders of magnitude larger than in analogous AFM experiments (Izrailev et al., 1997; Evans and Ritchie, 1997; Lu et al., 1998; Fisher et al., 2000; Isralewitz et al., 2001b).

The second stage of 1N11 elongation was further explored in four constant-force and one constant-velocity SMD simulations for the 1N0R structure containing only four identical ankyrin repeats (Mosavi et al., 2002). Constant-force SMD simulations were carried out using forces of 100 pN (sim8b), 200 pN (sim8c), 250 pN

(sim8d), and 300 pN (sim8e). Metastable lengths of  $\sim 70$  Å, 155–180 Å, and  $\sim 270$  Å were observed and suggest that multiple steps of 90–100 Å in the end-to-end distance are expected to accompany sequential unfolding of individual repeats.

The identification of intermediate states associated with unfolding of individual repeats in the constant-force simulations indicates that discernable force peaks may appear in sufficiently slow constant-velocity stretches. Indeed, a constant-velocity SMD simulation (Figure 6F; sim8h,  $v = 0.01$  Å/ps) clearly shows two force peaks ( $\sim 350$  pN) separated by  $\sim 97$  Å. The first force peak coincides with the separation of the last  $\alpha$  helix from the stack (Figure 6G). Separation of the other  $\alpha$  helix of the last repeat and the unfolding of these two detached  $\alpha$  helices follows at lower forces (Figure 6H). The second major force peak coincides with the separation of the second  $\alpha$  helix of the third repeat (Figure 6I), again followed by unfolding of the rest of the third repeat (Figure 6J). The detailed analysis of the rupture of key hydrogen bonds and van der Waals contacts is discussed in the supplemental data, Tables S1 and S2 and Figure S9.

These results indicate that polyankyrin domains respond to large forces in two phases. A first stage of elongation (the only stage for small forces) is characterized by changes in the overall curvature of the protein; a second stage of elongation is characterized by unfolding of individual repeats and rupture of the stack of repeats.

#### Partial Refolding of Ankyrin Domains

One may now ask what happens to unfolded ankyrin repeats when forces are switched off. To explore this behavior, we performed two additional simulations with the solvated 1N0R structure. First, a constant-velocity SMD simulation (Figure S10; sim8f) was carried out in which the last repeat and the first  $\alpha$  helix of the first repeat were completely unfolded. Then, velocities were

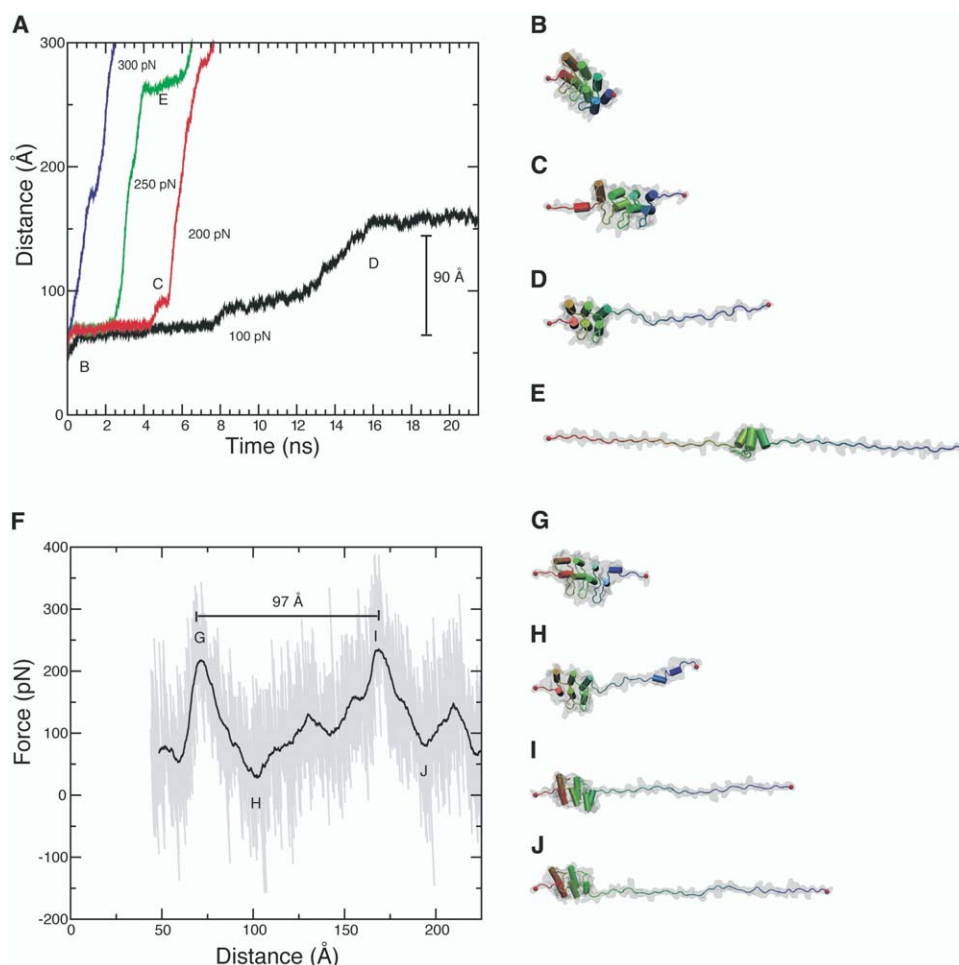


Figure 6. Unfolding of a Four-Ankyrin-Repeat Structure

(A) End-to-end distance for constant-force stretching at 100 pN (black, sim8b), 200 pN (red, sim8c), 250 pN (green, sim8d), and 300 pN (blue, sim8e).

(B–E) Snapshots of the initial equilibrated structure, of two intermediates, and of a final state as indicated through labels in (A).

(F) Force versus end-to-end distance (gray) for a constant-velocity SMD simulation ( $v = 0.01 \text{ \AA/ps}$ , sim8h). A running average using a 1 ns window is shown in black. Two major peaks separated by  $\sim 97 \text{ \AA}$  are clearly discernable.

(G–J) Snapshots for intermediate states during the constant-velocity SMD simulation. Repeats are color coded according to numbering, the first repeat red and the fourth repeat blue.

randomly reinitialized and the system was permitted to relax without force for 15.6 ns at constant temperature ( $T = 300 \text{ K}$ ; sim8g). The end-to-end distance decreased during the relaxation from  $\sim 203 \text{ \AA}$  to  $\sim 80 \text{ \AA}$ , showing a behavior compatible with a hydrophobic or entropic collapse (see Fernandez and Li, 2004, and references therein). The secondary structure as computed by STRIDE (Frishman and Argos, 1995; Figures S10C and S10D) reveals that partial refolding of the first  $\alpha$  helix occurred. Our mechanical model describing an overdamped spring (see Experimental Procedures) predicts a relaxation time of  $\tau \sim 3.7 \text{ ns}$  for the collapse.

How does the unfolded part of the protein behave after its collapse? The response to an external force  $F$  can be roughly described by a model of an entropic spring. For small forces, an entropic spring made of  $n$  freely jointed segments of length  $b$  would have a spring constant (Flory, 1969) of

$$k \sim \frac{3k_B T}{nb^2}, Fb \ll k_B T \quad (1)$$

The corresponding spring constant of a single unfolded ankyrin repeat containing 33 amino acids (three segments per amino acid of length  $\sim 1.4 \text{ \AA}$ ) is predicted to be  $\sim 6.5 \text{ mN/m}$ . The larger the number of ankyrin repeats unfolded, the smaller the effective spring constant.

The simulation of elongation due to large forces suggests that ankyrin stacks can actually act as safety elements (Howard and Bechstedt, 2004; Corey and Sotomayor, 2004). In response to extreme stimuli the structure unfolds one or more of its repeats. Then, the entropic collapse restores the end-to-end distance on a fast timescale while the unfolded domain still provides an appropriate elastic response to further upcoming stimuli.

## Discussion

The results of our simulations provide a close-up view of the elastic response of cadherin and polyankyrin do-

mains. While single cadherin domains respond with little change in end-to-end distance to moderate forces and require several hundred piconewtons to unfold, the two phases of elongation found for polyankyrin domains seem to be more suitable for a mechanical function as a hair-cell gating spring.

Indeed, the elastic response of polyankyrin domains in the first stage of elongation is well reproduced by a simple mechanical model of an overdamped linear spring. The source of the harmonic response was identified as the change in curvature of the overall structure for proteins containing 12, 17, and 24 repeats and, despite 2-fold elongations, did not involve changes in the secondary structure of the protein. A nonlinear response, with a slight increase of the associated spring constants for larger forces, may also be important for their function. A stiffer response is indeed expected for larger forces since compliance due to curvature is lost when the structure becomes straight, and the protein will eventually stretch up to a point where unfolding of the stack of repeats is required. The working extension of the hair-cell gating spring (10 to 20 nm) is in good agreement with the changes in the end-to-end distance observed for this first elongation phase in our SMD simulations of 24 and 17 ankyrin repeats. The predicted spring constants ( $\sim 5$  mN/m or less) are also in reasonable agreement with the gating-spring stiffness measured for hair-cell mechanotransduction ( $\sim 1$  mN/m). The rapid reversibility of the deformation induced in this first stage of elongation also supports the idea that polyankyrin domains are flexible mechanical elements. Simulations in vacuum (see [Supplemental Data](#)) confirm the astonishing flexibility and robustness of the ankyrin design as well as the suitability of mechanical models of linear springs invoked to describe the elastic response of polyankyrin domains.

The second phase of extension, characterized by unfolding and rupture of individual repeats, requires larger forces and longer times than elongation by change in the curvature. It needs yet to be established whether this conclusion is valid or not when the ankyrin repeats are stretched using smaller velocities or when they are bound to another protein. In any case, unfolding of individual repeats can be easily identified through force peaks in constant-velocity stretching (sawtooth pattern) or steps in constant-force stretching, as both force peaks and steps are separated by  $\sim 95$  Å. The end-to-end distance of unfolded polyankyrin domains could thus easily reach a maximum extension of  $\sim 2000$  Å or more while still conserving entropic stiffness and reversibility through entropic/hydrophobic collapse. Unfolding of individual repeats represents an attractive safety mechanism to protect against extreme stimuli.

All of these properties of the elastic response of polyankyrin domains strongly support the idea that ankyrin repeats in a transduction channel, rather than the tip link, are a more suitable candidate for the gating spring. The elastic response of our model of 17 ankyrin repeats of TRPA1 gives further support to this hypothesis. Moreover, the magnitude of the force peaks observed when stretching single cadherin domains, with or without  $\text{Ca}^{2+}$ , is significantly larger (by a factor of  $> 10$ ) than the force required to stretch or unfold multiple ankyrin repeats under the same simulation conditions. Although our simulations have not discarded changes of the

overall shape of multiple cadherin domains as a source of nonentropic elasticity, the immunoglobulin-like modules located in the tip link more likely act as a stiff cable, whereas ankyrin repeats located in the cytoplasmic domain of TRP channels act as soft nonentropic springs, much like the gating spring characterized biophysically (Corey and Hudspeth, 1983; Howard and Hudspeth, 1988).

Certainly, all of our results are predictions that need to be confirmed by experiments and through further simulations employing refined models and perhaps better crystallographic structures of both TRP ankyrin domains and cadherin 23. Moreover, key shortcomings of the molecular dynamics simulations must be considered, namely, the limiting nanosecond timescale and poor sampling. For instance, force peaks for unfolding ankyrin and cadherin are clearly overestimated due to the high velocities utilized to stretch the proteins: unfolding forces are more likely  $\sim 50$  pN for ankyrin and  $\sim 300$  pN for cadherin.

Further studies may also need to address how TRP ankyrin domains are attached to intracellular structures, how cadherin 23 interacts with the transduction channel and with itself (dimerization and interdigitiation), and what the molecular basis of ankyrin elasticity is. While we successfully characterized the ankyrin elastic response, the latter question remains open. Hydrophobic hydration may be an important source of elasticity, as pointed out in Li et al. (2001). However, our vacuum simulations excluded a major role of water and indicate an intrinsic source of elasticity related to van der Waals interactions between repeats. Indeed, the nonentropic elastic properties of ankyrin related to shape change in multiple repeats can be reproduced by harmonic springs defined through typical Lennard-Jones potentials acting in series.

Our findings have implications far beyond mechanotransduction. For instance, ankyrin repeats and ankyrin proteins have been thought to mediate protein-protein interactions. Do they also play a mechanical role? Indeed, the fact that spherocytosis in red blood cells is related to mutations in human ankyrin-R suggests, along with our results, that ankyrin proteins, and specifically, human ankyrin-R, may exert elastic forces. Ankyrin proteins may also play a role as mechanical isolators of nanomechanical motion of the cell wall (Pelling et al., 2004). Moreover, ankyrin proteins and ankyrin repeats associated with ion channels could act as sensors of temperature or ionic concentrations and, thereby, control gating of various sensory receptors (Schnatwinkel et al., 2004). The location of a calcium binding EF motif on the 17 ankyrin repeats of mmTRPA1 is very suggestive in that respect.

Our results have implications in the field of protein design as well. Indeed, ankyrin repeats have been successfully utilized as models for design of synthetic proteins and protein-folding studies (Binz et al., 2003; Binz et al., 2004; Mosavi et al., 2002; Mosavi et al., 2004; Mello and Barrick, 2004). Unfortunately, previous studies have focused on ankyrin-repeat proteins containing a rather small number of repeats with limited elasticity from curvature; additional properties may emerge from investigating extended repeat structures.

Finally, do other solenoid structures made out of repetitive units have elastic properties similar to those

observed for ankyrin? Proteins made from leucine-rich repeats (LRR); armadillo repeats; and heat repeats like internalin, decorin, importin- $\beta$ , exportin, clathrin, or catenin strikingly resemble the overall curved architecture of ankyrin. Do they also perform a mechanical function?

## Experimental Procedures

### Simulated Systems

Five different structures were simulated under various external conditions. The first derives from an extracellular domain of C-cadherin (PDB code 1L3W [Boggon et al., 2002]). Residues 102 to 214 forming the EC2 domain were included along with crystallographically resolved  $\text{Ca}^{2+}$  ions (unless otherwise stated). This domain is most similar in sequence to the consensus sequence of cadherin 23 (as revealed by sequence alignment performed using Clustal X [Gibson et al., 1994], data not shown), the component of the tip link in hair-cell bundles (Söllner et al., 2004; Siemens et al., 2004). The structure of EC2 will be referred to as 1L3W.

The second structure derives from the largest crystallographic structure of ankyrin repeats available to date, the 12 repeats of human ankyrin-R (PDB code 1N11 [Michaely et al., 2002]). The crystal structure contains repeats 13–24 of this protein along with 11 residues from its spectrin binding domain. The spectrin binding domain was truncated before simulation and the resulting structure is referred to as 1N11.

The third structure derives from a model of 24 repeats of human ankyrin-R (Michaely et al., 2002), which will be referred to below as MOD1. The model provided in Michaely et al. (2002) was constructed by examining the core contacts of the four helix bundles between individual repeats; bundles which most closely mirrored the core contact residues in individual bundles between repeats 1–13 were linked and distilled into a repeat stack (P. Michaely, personal communication). The resulting model of 24 repeats has been improved for the present study by threading the primary sequence onto repeats 1–13 using VMD (Humphrey et al., 1996) and by eliminating four extra residues in the fifth repeat (see Figure S3B). During the threading procedure, the old backbone atom coordinates were used for positions of backbone atoms of the new amino acids. The old coordinates of side chain atoms named identically to atoms of the new amino acid were used for positions of the new side chain atoms. The position of the remaining atoms was guessed using internal coordinates for each amino acid. A short minimization of 1000 steps in vacuo was performed utilizing NAMD (Kalé et al., 1999). From this resulted model MOD1.

The fourth structure derives from four identical engineered ankyrin repeats (PDB code 1N0R [Mosavi et al., 2002], see Figures 1A and 1C). Crystallographically resolved ions were not included in our simulations.

The last structure corresponds to a model of the ankyrin domains of the mouse channel TRPA1. This protein is likely to be part of the mechanotransduction apparatus in the inner ear of mammals (Corey et al., 2004). Unfortunately, no crystal structure is available. However, by analyzing its sequence using SMART (Letunic et al., 2004) and by performing a sequence alignment among the repeats themselves using Clustal X, 17 ankyrin repeats were identified and included in a structural model (see Figure S4). The model was built based on three assumptions: (1) the three-dimensional structure of individual ankyrin repeats, highly conserved despite variations in sequence, can be used as a template for the model; (2) extra residues according to the sequence alignment can be modeled as loops; and (3) all 17 repeats pack together in a single stack. Based on these assumptions, the primary sequence of the identified ankyrin repeats on TRPA1 was threaded onto repeats 8–24 of an equilibrated (sim3a, see below) configuration of MOD1. Residues missing according to the sequence alignment were eliminated from the structure. The threading procedure was followed as described above, and extra residues were included as simple loops. The resulting structure was minimized in vacuo for 1000 steps. The predicted structure, for which uncertainties are large, will be referred to below as MOD2.

The corresponding structures (1L3W, 1N11, MOD1, 1N0R, and MOD2) were spatially aligned such that the vector joining the  $\text{C}_\alpha$  atoms of the terminal residues was oriented along the  $x$  axis. The aligned proteins were then solvated (where applicable; see Table 1) using the VMD plugin Solvate. The VMD plugin Autoionize was used to place counterions to neutralize systems in the case of simulations that employed periodic boundary conditions and the PME method (see below) for electrostatic forces. Residues Asp, Glu, Lys, and Arg were assumed to be charged throughout the proteins. The protonation state of His residues was chosen by favoring the formation of evident hydrogen bonds.

### Molecular Dynamics

Molecular dynamics simulations were performed using the program NAMD 2.5 (Kalé et al., 1999) and the CHARMM27 force field for proteins (MacKerell et al., 1998) along with the TIP3P model for water molecules (Jorgensen et al., 1983).

A cutoff of 12 Å (switching function starting at 10 Å) for van der Waals interactions was assumed. Periodic boundary conditions were used in all but one simulation (sim6a); sizes of the periodic cell are indicated in Table 1. Distances between periodic images of the protein were greater than 20 Å in all cases. The particle mesh Ewald (PME) method was used to compute long-range electrostatic forces without cutoff in all simulations but one (sim6a). The density of grid points for PME was at least  $1/\text{Å}^3$  in all cases.

An integration time step of 1 fs was used, permitting a multiple time-stepping algorithm (Grubmüller et al., 1991; Schlick et al., 1999) to be employed in which interactions involving covalent bonds were computed every time step, short-range nonbonded interactions were computed every two time steps, and long-range electrostatic forces were computed every four time steps. The use of a multiple time-stepping algorithm allowed us to improve the performance of the simulations by a factor of two and, thus, reach the multianosecond timescale required to observe structural relaxation of the protein structures.

Langevin dynamics was utilized to enforce constant temperature ( $T = 300$  K) conditions (see Table 1). The Langevin damping coefficient was set to  $1 \text{ ps}^{-1}$ . This value was chosen to speed up conformational changes of the structures by reducing the solvent viscosity. Constant-pressure simulations (i.e., in the  $NpT$  ensemble) at 1 atm were conducted using the hybrid Nosé-Hoover Langevin piston method with a decay period of 200 fs and a damping-time constant of 100 fs.

### Analysis Tools and Mechanical Models

In order to monitor the structural deformation of the proteins, their root-mean-square deviation (rmsd) was computed using VMD (Humphrey et al., 1996) and coordinates saved every picosecond. The crystallographic structures served as the reference points when available; otherwise, the initial conformations were used as the reference point. Only positions of protein backbone atoms were compared. End-to-end distances were computed as the distance between the  $\text{C}_\alpha$  atom of the N-terminal residue and the  $\text{C}_\alpha$  atom of the C-terminal residue unless otherwise stated.

The average radius of curvature for structures 1N11 and MOD1 in different conformations was computed in three steps. First, a three-dimensional interpolation over the coordinates of  $\text{C}_\alpha$  atoms of residues located in position 7 (Figure 1D) was performed. The curve obtained from the interpolation and described by  $r(s)$  was then used to compute the radius of curvature  $R$  along the path length  $s$  according to

$$\frac{1}{R} = \frac{|\dot{r} \times \ddot{r}|}{|\dot{r}|^3} \quad (2)$$

where dots denote derivatives with respect to  $s$ . The third and final step consisted of averaging the values obtained along  $s$  to obtain an estimate of the overall curvature  $R$ .

Mechanical models of a simple spring in a viscous environment were utilized to rationalize the end-to-end distances monitored in our stretching and relaxation simulations. The equation governing the position  $y(t) = x(t) - x_0$  of a mass  $m$  connected to a spring of constant  $k$  and rest length  $x_0$  with damping coefficient  $\gamma$  used for the mechanical model is

$$m \frac{d^2y}{dt^2} + \gamma \frac{dy}{dt} + ky = F \quad (3)$$

where  $F$  is an external force acting also on  $m$ . The solution in the strong friction limit ( $m \sim 0$ ) for a constant stretching force  $F$  is

$$x(t) = x_0 + \frac{F}{k} \left( 1 - \exp\left(-\frac{kt}{\gamma}\right) \right) \quad (4)$$

which satisfies the initial ( $t = 0$ ) condition  $x = x_0$ . The corresponding solution describing relaxation in the force-free ( $F = 0$ ) case is

$$x(t) = x_0 + l \exp\left(-\frac{kt}{\gamma}\right) \quad (5)$$

where  $l$  represents the initial extension of the spring.

The solution of Equation 3 for an underdamped motion ( $\gamma < 4mk$ ) and constant stretching force  $F$  is

$$x(t) = x_0 + \frac{F}{k} \left[ 1 - \exp\left(-\frac{\gamma t}{2m}\right) \left( \frac{\gamma \sin(\omega t)}{\sqrt{4mk - \gamma^2}} + \cos(\omega t) \right) \right] \quad (6)$$

where  $\omega = \sqrt{k/m - \gamma^2/4m^2}$  and the solution satisfies the initial conditions  $x = x_0$  and  $dx/dt = 0$ .

The corresponding solution describing relaxation in the force-free case for initial conditions  $x = x_0 + l$  and  $dx/dt = 0$  is

$$x(t) = x_0 + l \times \exp\left(-\frac{\gamma t}{2m}\right) \left( \frac{\gamma \sin(\omega t)}{\sqrt{4mk - \gamma^2}} + \cos(\omega t) \right) \quad (7)$$

The mechanical models represented by Equations 4, 5, 6, and 7 were matched to the end-to-end distances monitored in our SMD simulations. From the match resulted values for  $m$ ,  $\gamma$ , and  $k$  when applicable, as summarized in Table 2. For the matching we employed the Levenberg-Marquardt algorithm.

#### Summary of Simulations

A summary of all simulations is presented in Table 1. Each solvated structure was equilibrated in the constant number, pressure, and temperature ( $NpT$ ) ensemble, and the resulting state was utilized to perform subsequent SMD simulations. Equilibration results for each structure and settings of different SMD simulations are discussed in the Supplemental Data.

#### Supplemental Data

Supplemental Data for this article can be found at <http://www.structure.org/cgi/content/full/13/4/669/DC1/>.

#### Acknowledgments

This work was partially supported by the National Institutes of Health (NIH P41 RR05969). The authors also acknowledge computer time provided by the National Science Foundation through the National Resource Allocation Committee grant MCA93S028. D.P.C. is an Investigator of the Howard Hughes Medical Institute. We thank P. Michaely for providing us with a model of human ankyrin-R, and members of the Theoretical and Computational Biophysics Group for helpful discussions. We thank Vann Bennett for bringing to our attention the possible elasticity of extended ankyrin repeats. Normal mode analysis (see Supplemental Data) was performed through the EInemo web interface (Suhre and Sanejouand, 2004). Plots and curve fits were prepared using xmgrace. The molecular images in this paper were created with the molecular graphics program VMD (Humphrey et al., 1996).

Received: December 21, 2004

Revised: February 10, 2005

Accepted: March 4, 2005

Published: April 12, 2005

#### References

- Bayas, M.V., Schulten, K., and Leckband, D. (2004). Forced dissociation of the strand dimer interface between C-cadherin ectodomains. *Mechanics and Chemistry of Biosystems* 1, 101–111.
- Bennett, V., and Chen, L. (2001). Ankyrins and cellular targeting of diverse membrane proteins to physiological sites. *Curr. Opin. Cell Biol.* 13, 61–67.
- Binz, H.K., Stumpp, M.T., Forrer, P., Amstutz, P., and Plückthun, A. (2003). Designing repeat proteins: well-expressed, soluble and stable proteins from combinatorial libraries of consensus ankyrin repeat proteins. *J. Mol. Biol.* 332, 489–503.
- Binz, H.K., Amstutz, P., Kohl, A., Stumpp, M.T., Briand, C.B., Forrer, P., Grütter, M.G., and Plückthun, A. (2004). High-affinity binders selected from designed ankyrin repeat protein libraries. *Nat. Biotechnol.* 22, 575–582.
- Boggon, T.J., Murray, J., Chappuis-Flament, S., Wong, E., Gumbiner, B.M., and Shapiro, L. (2002). C-cadherin ectodomain structure and implications for cell adhesion mechanisms. *Science* 296, 1308–1313.
- Bork, P. (1993). Hundreds of ankyrin-like repeats in functionally diverse proteins: mobile modules that cross phyla horizontally? *Proteins* 17, 363–374.
- Clapham, D.E. (2003). TRP channels as cellular sensors. *Nature* 426, 517–524.
- Corey, D.P. (2003). New TRP channels in hearing and mechanosensation. *Neuron* 39, 585–588.
- Corey, D.P., and Hudspeth, A.J. (1983). Kinetics of the receptor current in bullfrog saccular hair cells. *J. Neurosci.* 3, 962–976.
- Corey, D.P., and Sotomayor, M. (2004). Tightrope act. *Nature* 428, 901–902.
- Corey, D.P., García-Añoveros, J., Holt, J.R., Kwan, K.Y., Lin, S.Y., Vollrath, M.A., Amalfitano, A., Cheung, E.L.-M., Derfler, B.H., Duggan, A., et al. (2004). TRPA1 is a candidate for the mechanosensitive transduction channel of vertebrate hair cells. *Nature* 432, 723–730.
- Creighton, T.E. (1993). *Proteins*, second edition (New York: W.H. Freeman and Company).
- Evans, E., and Ritchie, K. (1997). Dynamic strength of molecular adhesion bonds. *Biophys. J.* 72, 1541–1555.
- Fernandez, J.M., and Li, H. (2004). Force-clamp spectroscopy monitors the folding trajectory of a single protein. *Science* 303, 1674–1678.
- Fisher, T.E., Marszalek, P.E., and Fernandez, J.M. (2000). Stretching single molecules into novel conformations using the atomic force microscope. *Nat. Struct. Biol.* 7, 719–724.
- Flory, P.J. (1969). *Statistical Mechanics of Chain Molecules* (New York: Interscience Publishers).
- Frishman, D., and Argos, P. (1995). Knowledge-based protein secondary structure assignment. *Proteins* 23, 566–579.
- Gao, M., Craig, D., Lequin, O., Campbell, I.D., Vogel, V., and Schulten, K. (2003). Structure and functional significance of mechanically unfolded fibronectin type III1 intermediates. *Proc. Natl. Acad. Sci. USA* 100, 14784–14789.
- Garcia, J.A., Yee, A.G., Gillespie, P.G., and Corey, D.P. (1998). Localization of myosin- $\text{I}\beta$  near both ends of tip links in frog saccular hair cells. *J. Neurosci.* 18, 8637–8647.
- Gibson, T., Higgins, D., and Thompson, J. (1994). Clustal X (Heidelberg, Germany: EMBL).
- Gillespie, P.G., and Walker, R.G. (2001). Molecular basis of mechanosensory transduction. *Nature* 413, 194–202.
- Gillespie, P.G., Wagner, M.C., and Hudspeth, A.J. (1993). Identification of a 120 kd hair-bundle myosin located near stereociliary tips. *Neuron* 11, 581–594.

- Groves, M.R., and Barford, D. (1999). Topological characteristics of helical repeat proteins. *Curr. Opin. Struct. Biol.* 9, 383–389.
- Grubmüller, H., Heller, H., Windemuth, A., and Schulten, K. (1991). Generalized Verlet algorithm for efficient molecular dynamics simulations with long-range interactions. *Mol. Simul.* 6, 121–142.
- Holt, J.R., Gillespie, S.K., Provance, D.W., Shah, K., Shokat, K.M., Corey, D.P., Mercer, J.A., and Gillespie, P.G. (2002). A chemical-genetic strategy implicates myosin-1c in adaptation by hair cells. *Cell* 108, 371–381.
- Howard, J. (2001). *Mechanics of Motor Proteins and the Cytoskeleton* (Sunderland, MA: Sinauer).
- Howard, J., and Bechstedt, S. (2004). Hypothesis: a helix of ankyrin repeats of the NOMPC-TRP ion channel is the gating spring of mechanoreceptors. *Curr. Biol.* 14, 224–226.
- Howard, J., and Hudspeth, A.J. (1988). Compliance of the hair bundle associated with gating of mechano-electrical transduction channels in the bullfrog's saccular hair cell. *Neuron* 1, 189–199.
- Howard, J., Roberts, W.M., and Hudspeth, A.J. (1988). Mechano-electrical transduction by hair cells. *Annu. Rev. Biophys. Chem.* 17, 99–124.
- Hudspeth, A.J. (1982). Extracellular current flow and the site of transduction by vertebrate hair cells. *J. Neurosci.* 2, 17–34.
- Hudspeth, A.J., and Corey, D.P. (1977). Sensitivity, polarity, and conductance change in the response of vertebrate hair cells to controlled mechanical stimuli. *Proc. Natl. Acad. Sci. USA* 74, 2407–2411.
- Humphrey, W., Dalke, A., and Schulten, K. (1996). VMD: visual molecular dynamics. *J. Mol. Graph.* 14, 33–38.
- Isralewitz, B., Baudry, J., Gullingsrud, J., Kosztin, D., and Schulten, K. (2001a). Steered molecular dynamics investigations of protein function. *J. Mol. Graph. Model.* 19, 13–25.
- Isralewitz, B., Gao, M., and Schulten, K. (2001b). Steered molecular dynamics and mechanical functions of proteins. *Curr. Opin. Struct. Biol.* 11, 224–230.
- Izrailev, S., Stepaniants, S., Balsera, M., Oono, Y., and Schulten, K. (1997). Molecular dynamics study of unbinding of the avidin-biotin complex. *Biophys. J.* 72, 1568–1581.
- Jorgensen, W.L., Chandrasekhar, J., Madura, J.D., Impey, R.W., and Klein, M.L. (1983). Comparison of simple potential functions for simulating liquid water. *J. Chem. Phys.* 79, 926–935.
- Kachar, B., Parakkal, M., Kurc, M., Zhao, Y., and Gillespie, P. (2000). High-resolution structure of hair-cell tip links. *Proc. Natl. Acad. Sci. USA* 97, 13336–13341.
- Kajava, A.V. (2002). What curves  $\alpha$ -solenoids? *J. Biol. Chem.* 277, 49791–49798.
- Kalé, L., Skeel, R., Bhandarkar, M., Brunner, R., Gursoy, A., Krawetz, N., Phillips, J., Shinozaki, A., Varadarajan, K., and Schulten, K. (1999). NAMD2: greater scalability for parallel molecular dynamics. *J. Comput. Phys.* 151, 283–312.
- Letunic, I., Copley, R.R., Schmidt, S., Ciccarelli, F.D., Doerks, T., Schultz, J., Ponting, C.P., and Bork, P. (2004). SMART 4.0: towards genomic data integration. *Nucleic Acids Res.* 32, D142–D144.
- Li, B., Alonso, D.O.V., Bennion, B.J., and Daggett, V. (2001). Hydrophobic hydration is an important source of elasticity in elastin-based biopolymers. *J. Am. Chem. Soc.* 123, 11991–11998.
- Li, L., Huang, H.H., Badilla, C.L., and Fernandez, J.M. (2004). Mechanical unfolding intermediates observed by single-molecule force spectroscopy in a fibronectin type III module. *J. Mol. Biol.* 345, 817–826.
- Lu, H., Isralewitz, B., Krammer, A., Vogel, V., and Schulten, K. (1998). Unfolding of titin immunoglobulin domains by steered molecular dynamics simulation. *Biophys. J.* 75, 662–671.
- Lux, S.E., John, K.M., and Bennett, V. (1990a). Analysis of cDNA for human erythrocyte ankyrin indicates a repeated structure with homology to tissue-differentiation and cell-cycle control proteins. *Nature* 344, 36–42.
- Lux, S.E., Tse, W.T., Menninger, J.C., John, K.M., Harris, P., Shalev, O., Chilcote, R.R., Marchesi, S.L., Watkins, P.C., Bennett, V., et al. (1990b). Hereditary spherocytosis associated with deletion of human erythrocyte ankyrin gene on chromosome 8. *Nature* 345, 736–739.
- MacKerell, A.D., Jr., Bashford, D., Bellott, M., Dunbrack, R.L., Jr., Evanseck, J., Field, M.J., Fischer, S., Gao, J., Guo, H., Ha, S., et al. (1998). All-hydrogen empirical potential for molecular modeling and dynamics studies of proteins using the CHARMM22 force field. *J. Phys. Chem. B* 102, 3586–3616.
- Main, E.R.G., Jackson, S.E., and Regan, L. (2003). The folding and design of repeat proteins: reaching a consensus. *Curr. Opin. Struct. Biol.* 13, 482–489.
- Mello, C.C., and Barrick, D. (2004). An experimentally determined protein folding energy landscape. *Proc. Natl. Acad. Sci. USA* 101, 14102–14107.
- Michaely, P., and Bennett, V. (1993). The membrane-binding domain of ankyrin contains four independently folded subdomains, each comprised of six ankyrin repeats. *J. Biol. Chem.* 268, 22703–22709.
- Michaely, P., Tomchick, D.R., Machius, M., and Anderson, R.G.W. (2002). Crystal structure of a 12 ANK repeat stack from human ankyrinR. *EMBO J.* 21, 6387–6396.
- Mosavi, L.K., Minor, D.L., and Peng, Z. (2002). Consensus-derived structural determinants of the ankyrin repeat motif. *Proc. Natl. Acad. Sci. USA* 99, 16029–16034.
- Mosavi, L.K., Cammett, T.J., Desrosiers, D.C., and Peng, Z. (2004). The ankyrin repeat as molecular architecture for protein recognition. *Protein Sci.* 13, 1435–1448.
- Pelling, A.E., Sehati, S., Gralla, E.B., Valentine, J.S., and Gimzewski, J.K. (2004). Local nanomechanical motion of the cell wall of *Saccharomyces cerevisiae*. *Science* 305, 1147–1150.
- Pickles, J.O., Comis, S.D., and Osborne, M.P. (1984). Cross-links between stereocilia in the guinea pig organ of corti, and their possible relation to sensory transduction. *Hear. Res.* 15, 103–112.
- Schlick, T., Skeel, R., Brünger, A., Kalé, L., Board, J.A., Jr., Hermans, J., and Schulten, K. (1999). Algorithmic challenges in computational molecular biophysics. *J. Comput. Phys.* 151, 9–48.
- Schnatwinkel, C., Christoforidis, S., Lindsay, M.R., Uttenweiler-Joseph, S., Wilm, M., Parton, R.G., and Zerial, M. (2004). The rab5 effector rabankyrin-5 regulates and coordinates different endocytic mechanisms. *PLoS Biol.* 151, e261. 10.1371/journal.pbio.0020261
- Sedgwick, S.G., and Smerdon, S.J. (1999). The ankyrin repeat: a diversity of interactions on a common structural framework. *Trends Biochem. Sci.* 24, 311–316.
- Shapiro, L., Kwong, P.D., Fannon, A.M., Colman, D.R., and Hendrickson, W.A. (1995). Consideration on the folding topology and evolutionary origin of cadherin domains. *Proc. Natl. Acad. Sci. USA* 92, 6793–6797.
- Sidi, S., Friederich, R.W., and Nicolson, T. (2003). NompC TRP channel required for vertebrate sensory hair cell mechanotransduction. *Science* 301, 96–99.
- Siemens, J., Lillo, C., Dumont, R.A., Reynolds, A., Williams, D.S., Gillespie, P.G., and Müller, U. (2004). Cadherin 23 is a component of the tip link in hair-cell stereocilia. *Nature* 428, 950–955.
- Söllner, C., Rauch, G.-J., Siemens, J., Geisler, R., Schuster, S.C., Müller, U., and Nicolson, T. (2004). Mutations in cadherin 23 affect tip links in zebrafish sensory hair cells. *Nature* 428, 955–958.
- Suhre, K., and Sanejouand, Y. (2004). ElNemo: a normal mode web-server for protein movement analysis and the generation of templates for molecular replacement. *Nucleic Acids Res.* 32, W610–W614.
- Walker, R.G., Willingham, A.T., and Zuker, C.S. (2000). A *Drosophila* mechanosensory transduction channel. *Science* 287, 2229–2234.
- Zhu, B., Chappuis-Flament, S., Wong, E., Jensen, I.E., Gumbiner, B.M., and Leckband, D. (2003). Functional analysis of the structural basis of homophilic cadherin adhesion. *Biophys. J.* 84, 4033–4042.